WILEY-VCH

DOI: 10.1002/ ((please add manuscript number))
Article type: Full Paper

Electrical Switching of Magnetization in the Artificial Multiferroic System $Co_{0.4}Fe_{0.4}B_{0.2}/BaTiO_3$: the Role of Magnetic Viscosity

*Lorenzo Baldrati, Christian Rinaldi, Alberto Manuzzi, Marco Asa, Stefano Bertoli, Lucia Aballe, Michael Foerster, Neven Biškup, Maria Varela, Matteo Cantoni, and Riccardo Bertacco**

L. Baldrati, Dr. C. Rinaldi, A. Manuzzi, M. Asa, S. Bertoli, Prof. M. Cantoni, Prof. R. Bertacco
Department of Physics, Politecnico di Milano, Via G. Colombo 81, Milano, 20133, Italy
E-mail: riccardo.bertacco@polimi.it
Dr. C. Rinaldi, Prof. R. Bertacco
IFN-CNR, Via G. Colombo 81, Milano, 20133, Italy

Dr. L. Aballe, Dr. M. Foerster
ALBA Synchrotron Light Facility, Carretera BP 1413, Km. 3.3, Cerdanyola del Vallès, Barcelona, 08290, Spain

N. Biškup, Prof. M. Varela
GFMC & Instituto Pluridisciplinar, Universidad Complutense de Madrid, Madrid, 28040, Spain
N. Biškup
Centro Nacional de Microscopía Electrónica, Universidad Complutense de Madrid, Madrid, 28040, Spain

Keywords: perpendicular magnetic anisotropy, magnetoelectric coupling, artificial multiferroics, magnetic viscosity

Abstract

Despite the huge amount of publications on artificial multiferroics, poor attention has been devoted to the role of magnetic viscosity in the electrically induced switching of the magnetization. In this paper we address this issue with reference to a novel multiferroic system displaying perpendicular magnetic anisotropy: the $Co_{0.4}Fe_{0.4}B_{0.2}/BaTiO_3$ bilayer. At room temperature, the $Co_{0.4}Fe_{0.4}B_{0.2}$ magnetic coercive field displays a hysteretic behavior, as a function of the voltage across the $BaTiO_3$ layer, with a 60% variation for complete reversal of the ferroelectric $BaTiO_3$ polarization. This is deployed to achieve the electric switching of the magnetization of individual $Co_{0.4}Fe_{0.4}B_{0.2}$ electrodes. Upon the $BaTiO_3$ polarization reversal under a magnetic bias field, the $Co_{0.4}Fe_{0.4}B_{0.2}$ layer jumps from an initial metastable state into the opposite magnetization state, with a characteristic switching time determined by magnetic viscosity. The magnetically assisted bipolar electric switching of the magnetization is demonstrated, via voltage pulses compatible with CMOS electronics, under uniform bias fields as low as 10 Oe.

1. Introduction

The electric control of magnetic properties has recently received great attention both from the fundamental and the technological points of view. Flipping the magnetization by an electric field represents a promising route towards high density and power saving integrated memory and logic devices. For instance, it would allow to overcome the main obstacle in miniaturization of magnetoresistive random-access memories (MRAM), i.e. the power dissipation during writing. [1–3] To this scope, recently there has been a renewed interest in strategies exploiting ion migration for controlling the magnetization. Huge magneto-ionic effects have been observed in inorganic devices due to oxygen ion migration towards or outwards the interface between an oxide and an ultrathin ferromagnetic layer with perpendicular to plane magnetic anisotropy.[4] Sizeable anisotropy variations were also found in electrolyte-solid systems upon

accumulation of charges with opposite polarity via ion migration.[5,6]In parallel, a great effort is put on the investigation of multiferroics, which would represent the materials of choice for the integrated electric control of magnetization. Unfortunately, a single phase material showing a sizeable interplay between ferroelectricity and ferromagnetism at room temperature has not been found yet. Instead, artificial multiferroic heterostructures, coupling ferroelectric (FE) and ferromagnetic (FM) materials with high Curie temperatures, are promising candidates to overcome the limitations of single phase materials.[7–9] The strain-induced spin reorientation transition, i.e. the reorientation of the magnetization from out of plane to in plane or vice versa, has been demonstrated in magnetic films on piezoelectric substrates.[10–13] This is an interesting approach but not well-suited for applications due to the expensiveness of piezoelectric single crystals and difficulties in integration. Sizable magnetoelectric effects have been reported at FE polymer - inorganic interfaces, as a result of the ferroelectric polarization inversion, but the integration of polymers with conventional electronics is not straightforward.[14] In the particular case of FE/FM heterostructures, electronic interfacial magnetoelectric effects can lead to fully reversible electrically-induced interfacial magnetic ordering transitions, as demonstrated for the epitaxial Co/Fe/BTO/$La_{0.7}Sr_{0.3}MnO_3$ system.[15] However, this effect is confined at the very interface, so that its use is limited to the case of devices such as hybrid ferroelectric and magnetic tunneling junctions, made of FM electrodes sandwiching a FE barrier, where the interfacial magnetization plays a major role.[16,17]

The voltage control of magnetic anisotropy in Ta/CoFeB/MgO heterostructures involved in magnetic tunnel junctions has been widely discussed in the framework of the electric writing of the magnetic information in MRAM devices.[18] Below a critical thickness, on the order of 1 nm, CoFeB displays perpendicular magnetic anisotropy (PMA). Sizable changes of the magnetic anisotropy can be achieved upon application of a few Volts across the MgO barrier, producing a modification of the interface hybridization.[19,20] Unfortunately, the electric fields

are very high, on the order of a few $MVcm^{-1}$, and can be highly detrimental for the barrier, thus reducing the device lifetime.

An alternative approach allowing to overcome this limitation consists in achieving the voltage control of the magnetic anisotropy in an artificial multiferroic, exploiting the effective electric field produced by polarization charges at the interface between a FM and a FE layer.[21] Voltages pulses of just a few volts can easily switch the dielectric polarization of relatively thick FE layers (up to hundreds of nm) and are associated to much lower electric fields, hence reducing the overall device aging. Furthermore, FE hysteresis provides an effective way to obtain non-volatile magnetoelectric coupling. However, so far just a few authors have studied the interplay between magneto-electric effects and magnetic viscosity, which ultimately determines the characteristic switching times, leaving the topic largely uncovered. [22]

In this paper we report on the electric control of the magnetic anisotropy in ultrathin CoFeB films displaying PMA, grown on an inorganic lead-free FE material, i.e. $BaTiO_3$ (BTO).[23] This novel artificial multiferroic system is fully compatible with semiconductor technology, thanks to the availability of industrial processes for growing $Ba_xSr_{1-x}TiO_3$ films on Silicon.[24–30] For CoFeB thickness below 1.3 nm, PMA is stabilized and the magnetic coercive field follows the ferroelectric hysteresis loop, with a maximum variation of 60% induced by full polarization reversal. This is used to demonstrate the magnetically assisted bipolar switching of the magnetization in CoFeB electrodes, requiring a magnetic bias field as low as 10 Oe and voltage pulses compatible with CMOS electronics. The FE switching shrinks the FM hysteresis loop, thus converting a metastable magnetization state at a given bias field into an unstable one. By consequence, a magnetization switching occurs, whose dynamic is governed by magnetic viscosity. Upon polarization reversal, a variation of the initial state relaxation time by about 4000% is found, for the minimum bias field ensuring a magnetic switching within 2 s from the FE switching. Faster switching times (below 1 ms) can be achieved at higher magnetic field bias, at the expense of the stability of the initial magnetic state.

2. Results and discussion

2.1. PMA in ultrathin CoFeB films on $BaTiO_3$

The first step of this work was the optimization of the growth parameters and thermal treatments leading to ultrathin CoFeB films with PMA on BTO. As PMA is an interfacial effect, it represents an ideal condition in view of the anisotropy modulation via accumulation of polarization charges at the CoFeB/BTO interface. We first synthesized $BaTiO_3$(100)/ $La_{0.7}Sr_{0.3}MnO_3$ (30) heterostructures (thicknesses in nanometres from now on) on $SrTiO_3$(001) substrates by pulsed laser deposition (PLD), on top of which we subsequently grew Ta(2.5)/CoFeB bilayers by magnetron sputtering. The $La_{0.7}Sr_{0.3}MnO_3$ (LSMO) layer serves as conductive bottom electrode for poling the BTO layer. Ta acts as protective layer but it also plays a fundamental role in stabilizing the PMA of CoFeB during the post-annealing. Details on the growth conditions can be found in the experimental section. Finally, a post-growth annealing of the whole stack, at 250°C for 15 minutes with an out of plane magnetic field of 4 kOe, was performed in vacuum to promote PMA. Scanning transmission electron microscopy (STEM) images were acquired in an aberration corrected JEOL JEM ARM200CF microscope operated at 200 kV and equipped with a Gatan Quantum electron energy-loss spectrometer (EELS). The STEM analysis of as-grown samples is reported in the Supporting Information (Figure S1), while here we concentrate on annealed samples displaying PMA. The stack composition was Ta(2.5)/CoFeB(1.1)/BTO(100)/LSMO(30)/STO. From STEM images reported in **Figure 1a**, layers appear flat and continuous over long lateral distances. LSMO and BTO layers are fully epitaxial, displaying the expected cube-on-cube growth along the (001) direction, while CoFeB and Ta are amorphous, exhibiting slightly rougher interfaces. Some deterioration of the BTO layer appears at the CoFeB/BTO interface, as revealed by the darker region just underneath CoFeB, where atoms are barely distinguishable. This is probably due to

the soft-etch process performed in the sputtering machine prior to CoFeB deposition or to some chemical interdiffusion. EELS elemental maps reported in **Figure 1b** show well defined layers. **Figure 1c** shows the averaged signals for B, Ti, Fe, Co and Ba across the stacking. The elemental signals decay across the interfaces in a fashion that is consistent with the Z-contrast images, with tails of Co, Fe and B into the BTO which denote a non atomically sharp interface. Note that a noticeable level of B signal, much larger than Co and Fe ones, is detected into the BTO layer. We cannot relate this fact directly to chemical interdiffusion of B into the BTO, as it could be due to artifacts during background subtraction in the BTO layer. The B *K* edge (used to produce this map) sits on top of the Ba $N_{2,3}$ edge, and hence background subtraction is a challenging task on the BTO/CoFeB interface. On the other hand, a tendency of B to diffuse into Ta after post annealing can be barely appreciated. Comparing the B signal with those of Co and Fe at the CoFeB/Ta interface, a spatial offset < 0.5 nm of the B tail extending in the Ta layer and a broader peak can be observed. The last finding is in agreement with previous studies, pointing to B interdiffusion and intermixing at the CoFeB/Ta interface as a key mechanism to promote the formation of PMA in ultrathin CoFeB films sandwiched between oxides and Ta.[31,32] Our data, however, suggest that also the intermixing at the CoFeB/BTO interface could be relevant for the stabilization of PMA.

The magnetic anisotropy of the CoFeB layer was studied by Vibrating Sample Magnetometry (VSM) on Ta(2.5)/$Co_{0.4}Fe_{0.4}B_{0.2}$(t)/BTO(001)/STO samples annealed at 250°C in a magnetic field of 4 kOe perpendicular to the sample surface. The CoFeB thickness (*t*) was varied between 1.1 and 1.6 nm, in the region where the spin reorientation transition takes place in analogous systems.[20] LSMO was not included in the stack to avoid its magnetic contribution to VSM measurements, after having verified (data not shown) that its influence on CoFeB magnetic properties is negligible. This is largely expected from the low LSMO-STO lattice mismatch (the in plane tensile strain estimated from bulk lattice parameters is about -0.8 %) and large

BTO thickness (100 nm) over which strain is certainly released by dislocations.[33] As grown CoFeB films are magnetically isotropic in the plane, while PMA appears only after post-annealing, below a critical thickness. The effective anisotropy constant (K_{eff}) has been evaluated from the hard-axis hysteresis loops measured for each thickness, according to the Stoner-Wohlfarth model: $K_{eff} = \mu_0 M_s H_a/2$, where M_s is the saturation magnetization and H_a the anisotropy field, i.e. the field at which the magnetization saturates along the hard axis. As usual, K_{eff} is assumed negative for in-plane and positive for out-of-plane anisotropy. The product of the effective anisotropy by the film thickness ($K_{eff}\,t$) is reported in **Figure 2a** as a function of the CoFeB thickness (t). The spin reorientation transition is clearly visible at about 1.3 nm. According to the loops for the in-plane (M_{IP}) and out-of-plane (M_{OP}) components of the magnetization reported in **Figure 2b and 2c**, below 1.3 nm films display PMA while above this thickness the shape anisotropy overwhelms the interfacial anisotropy and the magnetization reorients in plane. This value is comparable to that found in Ta/CoFeB/MgO multilayers, thus signaling that the growth on BTO does not alter the CoFeB properties.[20] We separate interface and volume contributions to the effective anisotropy constant by fitting our data with the phenomenological formula: $K_{eff} \cdot t = K_V \cdot t + K_i$.[34] The volume ($K_v$) and interface ($K_i$) anisotropy constants turn out to be, respectively, -1067 ± 77 kJ m^{-3} and 1.4 ± 0.1 mJ m^{-2}.

To better investigate the magnetic properties of $Co_{0.4}Fe_{0.4}B_{0.2}$ films with PMA, X-ray Photo-Electron Emission Microscopy (X-PEEM) measurements were carried out at the CIRCE beamline of ALBA synchrotron.[35] A space-resolved X-Ray Magnetic Circular Dichroism (XMCD-PEEM) map, acquired at the Fe L_3 edge (706.5 eV) from a sample with CoFeB thickness of 1.1 nm, is included in the inset of Figure 2a (see Figure S2 and related discussion in the Supporting information for further details). Some residuals magnetic worm-like domains, typical of systems with PMA, are clearly visible at remanence after application of 110 Oe. This underlines the intrinsic tendency of this system to nucleate magnetic domains, whose wall

depinning and propagation are crucial to understand magnetization reversal and magnetic relaxation phenomena in our films.

2.2 Micro-capacitors fabrication and characterization

To investigate magneto-electric coupling we fabricated arrays of micro-capacitors suitable for the electric poling of BTO during magneto optical Kerr effect measurements (MOKE), as illustrated in **Figure 3a**. We adopted a top-top configuration, where two BTO capacitors are connected in series through the conducting LSMO bottom electrode. The fabrication has been carried out on annealed Ta/CoFeB/BTO/LSMO/STO(001) stacks by means of optical lithography, Ion Beam Etching, deposition of a SiO_2 capping layer and Au/Ti contacts. Arrays of capacitors with 100x70 μm^2 area have been obtained, with a sizable portion of the top Ta/CoFeB electrode clear of the thick Au/Ti contacts, thus allowing to probe the underlying CoFeB layer by MOKE measurements.

The ferroelectric properties of the micro-capacitors have been investigated with the virtual ground method using a TF Analyzer 2000 from AixACCT Co. equipped with ferroelectric module. The room temperature FE hysteresis loops, recorded with Dynamic Leakage Current Compensation and Positive-Up Negative-Down (PUND) methods, are reported in Figure 3a and 3b, respectively.[36] From now on, all reported voltages correspond to the drop across two adjacent capacitors connected in series, which is roughly twice the voltage drop across a single capacitor. The devices show the expected ferroelectric behavior, with a nominal saturation polarization of about 30 $\mu C\ cm^{-2}$ measured in the dynamic mode but a modest value of remanent polarization (3 $\mu C\ cm^{-2}$), as seen from PUND measurements. The latter must be compared with the typical value of 10 $\mu C\ cm^{-2}$ we have obtained in similar capacitors with LSMO/BTO/Fe structure.[15] In the present case, the reduced polarization is mainly ascribed to the soft-etch of the BTO/LSMO/STO template, performed in the sputtering machine before the CoFeB

deposition. As a matter of fact, the removal of contaminants arising from exposure to the atmosphere revealed to be essential to achieve sizable magnetoelectric coupling. In perspective, the deterioration of the FE properties could be eliminated by using a dedicated machine for in-situ growth of both the template and the Ta/CoFeB bilayer.

Figure 3d reports the position of the current peak in PUND measurements, assumed as representative of the coercive voltage, as a function of the frequency of the train of pulses.[36] The coercive voltage decreases from 8 V at 1 kHz to less than 2 V at the lowest frequency probed (0.01 Hz). Similarly to what is observed in BTO single crystals[37] and in other ferroelectric thin films,[38–40] this is the effect of the rate-dependent nucleation and propagation of ferroelectric domains, which limits the polarization switching time and determines a viscous behavior [41] As a matter of fact the experimental points are well fitted with the Merz law[37] (see continuous line in Figure 3d) describing the thermal activation of the domain wall motion: $\nu = \nu_0 \exp(\alpha/V_c)$, where ν is the electric field frequency, V_c the coercive voltage and α the activation voltage. It is worth noting that the electric field applied during the magneto-electric measurements described in the next section are essentially static. Thus any observed magneto-electric phenomenon linked to the ferroelectricity of $BaTiO_3$ is connected to the low frequency regime of Figure 3d, where the coercive voltage is below 2 V.

2.3 Magneto-electric coupling

Figure 4 summarizes the results of MOKE measurements performed at different applied voltages (V) across the micro-capacitors (see the experimental section for details). From now on, positive V means that the voltage applied to the pad illuminated by the laser is positive with respect to the second electrode, i.e. the FE polarization points downwards underneath the CoFeB electrode under measurement. Note that the LSMO bottom layer displays a clear easy-plane anisotropy, so that polar loops presented in the following only reflect the CoFeB magnetic

properties (see Figure S4 and related discussion in the Supporting Information). The two hysteresis loops of Figure 4 show a huge voltage modulation of the magnetic coercive field (H_c): from 56 Oe for positive bias (+ 7 V, bottom right inset) to 35 Oe for negative bias (-7 V, top left inset), with a relative variation of about 60%. Noteworthy, H_c displays a hysteretic behavior as a function of the applied bias (see main panel of Figure 4) which is fully consistent with the low-frequency FE behavior discussed above. As a matter of fact, the transition between the low and high magnetic coercive field occurs at about 1 V, in agreement with a FE coercive voltage lower than 2 V at very low frequency (see Figure 3d). Even though data reported in Figure 4 have been collected under application of continuous voltages, in order to suppress any drift, the FE remanence ensures the stability of the low and high coercive states upon removal of the applied voltage. This is shown in Figure 4b, where only a small decay of the coercive field, on the order of 10%, is observed 2400 s after switching the BTO polarization with a 1 s long voltage pulse of +2 V. Distinct states of magnetic anisotropy can be written via voltage pulses, thus allowing for the non volatile electric reconfiguration of the magnetic properties of the CoFeB electrodes.

Spurious effects arising from current-induced heating can be ruled out by looking at the symmetry of the coercive field variation with respect to the applied voltage. In fact, even though the leakage current density in these devices was relatively high (J = 13 A/cm^2 at 5 V), the coercive field is an odd function with respect to the applied voltage (Figure 3a), while Joule heating would produce an even behavior. Analogously, we can exclude strain-mediated magneto-electric effects arising from the piezoelectric nature of BTO. First, strain would give an even contribution.[42] Second, the BTO film is epitaxially grown on LSMO/STO(001), so that clamping from the substrate inhibits possible inverse magnetostrictive phenomena.[16] Finally, also ion migration can be ruled out because we observe a sudden change of H_c upon voltage application, at variance with the much slower time evolution of the magnetic anisotropy (over a time-scale of minutes) expected in case of electro-migration.[4] As a matter of fact, our

data point to a purely electric nature of the observed magneto-electric coupling, in strict analogy with the case of voltage controlled magnetic anisotropy for the MgO/CoFeB system.[43] The sign of the effect is the same, as H_c increases for positive bias voltage, i.e. for the electric field pointing out of the CoFeB electrode. This suggests that the modulation of PMA could be related, also in the present case, to the change of the interfacial hybridization between 3*d* states of CoFeB and O *2p* orbitals from BTO, induced by the interfacial electric field arising from FE polarization charges of BTO. On the other hand we exclude that the increase of the magnetic coercive field can be related to a higher concentration of pinning sites connected to FE domain walls. If this was the case, the magnetic coercive field should peak at the FE coercive field, [13] while in our case it follows the FE hysteresis loop and depends on the sign of FE polarization. The coercive field increase at positive applied voltage is most probably connected to the increase of both the domain nucleation energy and the depinning field for the domain walls (DW). As a matter of fact the rounded shape of the magnetic hysteresis loops and their finite slope at the coercive field, point to a mechanism of magnetization reversal involving the thermally activated nucleation of many domains with opposite magnetization, in nice agreement with the XPEEM image of Figure 2. As both the nucleation energy barrier and the DW depinning field are expected to increase with the PMA strength, the magnetization reversal is delayed and the coercive field increases.[44,45] The entity of the effect (60% variation of the coercive field) is remarkable and is obtained upon application of just 2 V across a couple of capacitors, each one with a BTO thickness of 100 nm. Even though the modulation is slightly lower than what reported in case of CoFeB/MgO tunneling junctions, the use of much lower electric fields across the oxide layer (10 $mV \cdot nm^{-1}$ across BTO, to be compared with the typical value of 200 $mV \cdot nm^{-1}$ across thin MgO tunneling barriers) could improve the devices endurance.[19]

In **Figure 5** we report on the electrically induced double flip of the magnetization (up-down-up) in micro-capacitors, as monitored by micro-MOKE. The general idea is depicted in

panel 5a. Starting from a high coercivity magnetic state of the FM, the system is biased with a magnetic field in between the high and low coercive fields, corresponding to the initial state A. When the hysteresis loop shrinks, the state A becomes unstable and the system jumps into the new stable state B with opposite magnetization.[46] Figure 5b shows how this scheme has been implemented in the CoFeB/BTO system. First we set a high coercivity state (red loop in the top panel of Figure 5b) with a voltage V_S= +4 V and we magnetize the sample upwards (M_{OP}/M_S=+1). Then we prepare an initial state A, by application of a negative magnetic bias field H_b. Upon reversal of the FE polarization via application of the flip voltage V_f = -4 V, the CoFeB layer is turned into a low coercive state (black loop of the second panel in Figure 5b), so that the system jumps in a downwards magnetization state (see the vertical A-B transition in Figure 5). Interestingly enough, the jump happens also for smaller values of H_b, not in between the low and high magnetic coercive fields, down to a critical value H_b^-= -23 Oe which corresponds to the vertical transition A'B' in Figure 5b. This deviation from the ideal scheme of panel 5a is connected to the magnetic viscosity of the CoFeB layer, and will be carefully discussed in the next section. To obtain the opposite switching, a positive voltage (V_s = +4V) is first applied in order to increase the coercivity (state C') and then the bias magnetic field is reversed (H_b= +28 Oe). The system goes into the state D', from which the down-up magnetic flip (D'-E') is activated by switching the voltage to negative values (V_f = -4 V). Higher positive magnetic fields can be used to set a transition like that starting from D, within the limit imposed by the need of starting from a stable enough initial state, so that the switching is effectively electrically activated. The occurrence of the magnetization flip was checked by sweeping the magnetic field to positive or negative values while acquiring the MOKE signal, as shown with blue line in the second and fourth panel of Figure 5b.

Symmetry considerations impose the use of an auxiliary bipolar magnetic bias field to achieve reversible switching. Its sign determines the sense of the flip (up-down or down-up), while its entity must be properly chosen in order to ensure a reliable and fast operation. As already

pointed out, there exists a range of values of H_b allowing for the magnetic flip. With reference to Figure 5b the up-down (down-up) electrically assisted flip of the magnetization can be achieved for all H_b values setting an initial state between A' and A (D and D'). We have systematically determined the minimum value of H_b ensuring the magnetic flip of the magnetization within 2 s after the voltage switching, from the positive value ($-V_f$) to the negative value (V_f), as a function of V_f. The corresponding values H_b^- (H_b^+) for the up-down (down-up) magnetic transitions are reported in Figure 5c, where we also show the coercive field values (H_c^-, H_c^+) in the low coercive state obtained upon application of V_f. The shaded grey areas correspond to the "anomalous" transitions for bias field lower than the magnetic coercive field in the low coercive state, while the peculiar A' and D' states discussed in Figure 5b are marked with green dots. Noteworthy, the modulus of both $H_c^{\pm}$ and $H_b^{\pm}$ decreases for high negative bias voltages, with $|H_b^{\pm}|$ reaching a minimum of about 10 Oe for an applied voltage V_f = -16V, which was the maximum voltage sustainable by the micro-capacitors. This is not surprising for the non-ideal ferroelectric behaviour found in our devices, whose remanence polarization is only 3 $\mu C \cdot cm^{-2}$, to be compared with the nominal saturation value of 30 $\mu C \cdot cm^{-2}$ for BTO. Even though the FE coercive voltage is on the order of 2 V, larger surface charge densities are expected when increasing the voltage modulus above this value. The modulation of the magnetic anisotropy is more efficient at large negative voltages and both $H_c^{\pm}$ and $H_b^{\pm}$ decrease. Noteworthy, data in Figure 5c point to the possibility of using very low bias magnetic fields to assist the electric switching. This is crucial in view of the application of the CoFeB/BTO system to achieve the electric control of the magnetization of single FM elements on a chip, all exposed to a low uniform magnetic bias field but individually addressed by voltage pulses.

2.4 Switching times and magnetic viscosity

As anticipated above, the apparent experimental deviation from the ideal scheme of magnetic flip reported in Figure 5a can be explained taking into account the magnetic viscosity of the CoFeB layer. Furthermore, viscosity is the key phenomenon for understanding the dynamics of the switching and its connection to the bias field. As a matter of fact the switching time of the magnetization can be viewed as the sum of the ferroelectric switching time and of the relaxation time of the magnetic metastable states created upon application of V_f. While the FE switching time for BTO can be very fast, e.g. few tens of nanosecond in BTO crystals at 100 kV/cm and 0.1 ps in BTO thin films deposited by PLD,[47,48] the magnetic relaxation time (τ) is much longer and determines the overall switching time. Obviously, τ strongly depends on the metastability of the initial state selected via H_b, so that the crucial role of the bias field in determining the dynamics of the magnetic flip is easily understood.

To shed light on these aspects we have investigated the magnetic viscosity of CoFeB films on BTO, by measuring the dependence of the magnetic coercive field on the sweep rate of the external field applied during MOKE measurements.[49] In **Figure 6a**, it is seen that the coercive field increases from 25 Oe to 47 Oe when the sweep rate varies from 0.1 Oe/s to 40 Oe/s. The experimental logarithmic shape of Hc vs the sweep-rate is a clear fingerprint of magnetic viscosity. [Ref chapter Ferré] At high sweep rate the field variation is too fast with respect to the typical relaxation times of the system, connected to the finite activation barriers to be overcome during magnetization reversal. Thus the measured loop is made of a sequence of metastable states which could not be observed in case of slower sweep rates. The effective coercive field, measured by MOKE, increases at high sweep rates,[50] as the magnetization lags behind the applied magnetic field. These findings easily explain the apparent deviation of experimental data in Figure 5b from the ideal case of panel 5a. In fact, for the hysteresis loops of Figure 5 and the preparation of the initial states for the magnetic flip, a magnetic field sweep rate of 25 Oe/s was used, while the lowest bias fields $H_b^{\pm}$ have been determined as those

ensuring a flip within 2 s. This means that the hysteresis loops of Figure 5 are the right ones to be considered for the initial state of the transition, while for the final state we should consider loops with a coercive field which is about half of that reported in Figure 5, according to data in Figure 6. Thus even the lowest bias fields $H_b^{\pm}$ satisfy the general requirement of being comprised between the low and high magnetic coercive fields set by applied voltages.

The second relevant effect of magnetic viscosity is the finite relaxation time of metastable magnetic states, as shown in Figure 6b. If an initial "up" state of the magnetization is prepared and a negative (downwards) magnetic field H_b is applied, the system will "indefinitely" stay in the up state for low fields (blue dots in Figure 6b, H_b= -10 Oe) or will flip towards a down magnetization state in a characteristic relaxation time which decreases when H_b becomes more negative (see red and black curves in Figure 6b). In this framework the electrically induced magnetic switching shown in Figure 5 arises from the decrease of the magnetic relaxation time at a fixed magnetic bias, induced by the reversal of the ferroelectric polarization. This is clearly shown in **Figure 7a**, where we report the magnetic relaxation curves measured at fixed H_b= -22 Oe for ±7 V. For -7 V the magnetic flip is much faster than for +7 V, in agreement with the fact that for negative voltages the hysteresis loop shrinks and the instability of the initial state of the magnetic transition is increased. By inspection it is evident that an initial fast drop of the magnetization takes place, followed by a much slower decay which fully accomplishes the switching. There is a clear deviation from the logarithmic law describing magnetic relaxation curves in case of a flat distribution of energy barriers or relaxation times (see Figure S4 in the Supporting Information). As a matter of fact the decay can be fitted using only two exponential decay functions, in agreement with what is predicted in case of systems where nucleation plays a major role during magnetization reversal. [Libro Ferrè] Our CoFeB films display two distinct activation energy barriers, possibly associated to a granular composition of the film with two dominant grain sizes or to distinct energy barriers during the nucleation - propagation of domain walls like those seen in the inset of Figure 2a (see the Supporting Information for further

details). By plotting the time constant of the fast component (τ_F) at fixed H_b= -22 Oe as a function of the voltage applied across the capacitor, we found the characteristic hysteretic behaviour reported in Figure 7b, with a relative variation of τ_F on the order of 4000%. The relaxation time follows the FE polarization of BTO, like the magnetic coercive field does, thus underlining the connection between relaxation time and coercivity.[51] Coming back to the issue of the influence of the magnetic bias field on the switching time, it turns out that, at fixed voltage V_f, the minimization of H_b down to the limit value $H_b^{\pm}$ has the drawback of a corresponding increase of the switching time (see Figure 6). As a matter of fact $H_b^{\pm}$ have been experimentally defined as the lowest bias fields for which a magnetic flip can be electrically induced within an observation window of 2 s. This roughly corresponds to the situation of Figure 7, as -22 Oe is very close to H_b^-, according to Figure 5c, and the time constant of the fast decay for -7 V is τ_F^- = 2 s. In order to reduce the switching time, H_b must be increased but there is obviously an upper limit for H_b: we need a stable enough initial state in the high coercive state (for positive voltage), so that the system does not relax before the application of the negative voltage pulse. In other words, the ratio (τ_f^+ / τ_f^-) between the relaxation times for positive and negative voltage at fixed H_b must be greater than a threshold value chosen according to the specific application. For optimum values of H_b between $H_b^{\pm}$ and $H_c^{\pm}$, relaxation times in the initial state (τ_f^+) on the order of a few seconds and flipping times below the time resolution of our experimental setup (1 ms) can be obtained. This preliminary analysis definitely points to the need of minimizing magnetic viscosity in order to achieve faster switching times.

3. Conclusion

In this paper we report on the electric modulation of the perpendicular magnetic anisotropy in CoFeB ultrathin films grown on $BaTiO_3$(001). Upon reversal of the ferroelectric polarization, a 60% modulation of the coercive field is achieved. This is used to demonstrate the magnetically assisted bipolar electric switching of the magnetization, exploiting the fact that the shrinking of

the hysteresis loop induces the instability of the initial magnetic state. Uniform bipolar magnetic bias fields as low as 10 Oe are applied to the entire chip, while the flip of a single magnetic element is selectively activated by a localized voltage pulse. The magnetic relaxation times of the CoFeB film are strongly modulated by the ferroelectric polarization of BTO. This has a deep impact on the characteristic switching times achievable during the electrically induced magnetic flip, as the switching time roughly corresponds to the relaxation time of the metastable state created upon reversal of the ferroelectric polarization. Our results point out that there exists an optimum value of the bias magnetic field to be used to assist the switching: not too low to fasten the magnetic transitions but not too large in order to guarantee the stability of the initial states and prevent unintentional flip in magnetic elements non electrically addressed by the electric field. This work sheds light on the mechanisms of magnetic switching in artificial multiferroic systems, crucial for application in real spintronic devices.

4. Experimental Section

Sample growth. We used single-crystal STO(001), 10x10 mm substrates, with a r.m.s. roughness < 0.1 nm (CrysTec Gmbh). Epitaxial BTO(100 nm)/LSMO(30 nm) bilayers were grown by Pulsed Laser Deposition (PLD) using a quadrupled Q-switched Nd:YAG laser (λ= 266 nm) operated at a repetition rate of 2 Hz. For LSMO we used a fluence of 5.2 J/cm^2 in a O_2 pressure of 0.22 Torr and sample temperature of 730 °C. For BTO we adopted a lower fluence of 2.2 J/cm^2 in a O_2 pressure of 0.02 Torr and growth temperature of 640 °C, according to a previous optimization for this material.[52] At the end of the deposition, we performed a post annealing (30 min at 600 °C, O_2 pressure of 760 Torr). Further details about the PLD setup are reported elsewhere.[53] The samples were then transferred ex-situ in a magnetron sputtering system (AJA ATC Orion8), where we grew the CoFeB/Ta bilayer in DC mode, after a soft etch in Ar plasma for 30 s to clean the surface after the exposure to air. The base pressure of the sputtering chamber was better than 1×10^{-8} Torr.

Magnetic characterization. A μ-MOKE setup was specifically developed to perform the magneto-optical characterization of the micro-capacitors. Polar MOKE ellipticity loops were acquired focusing a laser diode (λ= 635 nm), with a beam spot down to a 10-30 μm diameter, on the Ta/CoFeB pads and simultaneously applying a bias voltage across two identical micro-capacitors, as schematically shown in Figure 3a. The positioning of the device in front of the beam was achieved by a triaxial micrometric stage and controlled by a camera showing both the sample and the laser spot at the same time. The magnetic field was generated by a pair of coils. A photoelastic modulator (PEM) operating at 50 kHz was used to modulate the beam polarization and the signal was demodulated by a lock-in amplifier at the same frequency in order to obtain Kerr ellipticity.

X-ray Photoemission Electron Microscopy (X-PEEM). measurements were carried out at the spectroscopic PEEM-LEEM endstation of CIRCE beamline at the ALBA Synchrotron Light Facility in Barcelona (Spain). The beamline provides a highly focused beam of polarized photons in the soft X-ray range (100−2000 eV) with a 16° angle of incidence respect to the plane of the sample and is equipped with an Elmitec SPELEEM setup (type LEEM III).[35]

Supporting Information
Supporting Information is available from the Wiley Online Library or from the author.

Acknowledgements
We gratefully acknowledge financial support from Fondazione Cariplo via the project Magister (Project No. 2013-0726) and from Italian Ministry of Research via the project FIRB OSSIDI NANOSTRUTTURATI: MULTI-FUNZIONALITA' E APPLICAZIONI (RBAP115AYN). We wish to thank M. Leone and L. Martinelli for skillful technical assistance.

Received: ((will be filled in by the editorial staff))
Revised: ((will be filled in by the editorial staff))
Published online: ((will be filled in by the editorial staff))

REFERENCES

[1] M. Bibes, *Nat. Mater.* **2012**, *11*, 354.

[2] J. Ma, J. Hu, Z. Li, C. W. Nan, *Adv. Mater.* **2011**, *23*, 1062.

[3] M. Bibes, A. Barthélémy, *Nat. Mater.* **2008**, *7*, 425.

[4] U. Bauer, L. Yao, A. J. Tan, P. Agrawal, S. Emori, H. L. Tuller, S. Van Dijken, G. S. D. Beach, *Nat. Mater.* **2015**, *14*, 174.

[5] M. Weisheit, S. Fähler, A. Marty, Y. Souche, C. Poinsignon, D. Givord, *Science* **2007**, *315*, 349.

[6] J. Jeong, N. Aetukuri, T. Graf, T. D. Schladt, M. G. Samant, S. S. P. Parkin, *Science* **2013**, *339*, 1402.

[7] C. A. F. Vaz, *J. Phys. Condens. Matter* **2012**, *24*, 333201.

[8] N. A. Spaldin, S. Cheong, R. Ramesh, *Phys. Today* **2010**, *63*, 38.

[9] W. Eerenstein, M. Wiora, J. L. Prieto, J. F. Scott, N. D. Mathur, *Nat. Mater.* **2007**, *6*, 348.

[10] N. A. Pertsev, *Phys. Rev. B* **2008**, *78*, 212102.

[11] W.-C. Tsai, S.-C. Liao, K.-F. Huang, D.-S. Wang, C.-H. Lai, *Appl. Phys. Lett.* **2013**, *103*, 252405.

[12] M. Weiler, A. Brandlmaier, S. Geprägs, M. Althammer, M. Opel, C. Bihler, H. Huebl, M. S. Brandt, R. Gross, S. T. B. Goennenwein, *New J. Phys.* **2009**, *11*, 013021.

[13] S. Brivio, D. Petti, R. Bertacco, J. C. Cezar, *Appl. Phys. Lett.* **2011**, *98*, 092505.

[14] A. Mardana, S. Ducharme, S. Adenwalla, *Nano Lett.* **2011**, *11*, 3862.

[15] G. Radaelli, D. Petti, E. Plekhanov, I. Fina, P. Torelli, B. R. Salles, M. Cantoni, C. Rinaldi, D. Gutiérrez, G. Panaccione, M. Varela, S. Picozzi, J. Fontcuberta, R. Bertacco, *Nat. Commun.* **2014**, *5*, 3404.

[16] G. Radaelli, D. Petti, M. Cantoni, C. Rinaldi, R. Bertacco, *J. Appl. Phys.* **2014**, *115*, 172604.

[17] M. Asa, L. Baldrati, C. Rinaldi, S. Bertoli, G. Radaelli, M. Cantoni, R. Bertacco, *J. Phys. Condens. Matter* **2015**, *27*, 504004.

[18] R. Bertacco, M. Cantoni, *in Ultra-High-Density Magnetic Recording: Storage Materials and Media Design*; Varvaro, G.; Casoli, F., Eds.; Pan Stanford Publishing (in press), 2016.

[19] M. Endo, S. Kanai, S. Ikeda, F. Matsukura, H. Ohno, *Appl. Phys. Lett.* **2010**, *96*, 212503.

[20] S. Ikeda, K. Miura, H. Yamamoto, K. Mizunuma, H. D. Gan, M. Endo, S. Kanai, J. Hayakawa, F. Matsukura, H. Ohno, *Nat Mater* **2010**, *9*, 721.

[21] P. V Lukashev, J. D. Burton, S. S. Jaswal, E. Y. Tsymbal, *J. Phys. Condens. Matter* **2012**, *24*, 226003.

[22] A. Mardana, S. Ducharme, S. Adenwalla, *J. Appl. Phys.* **2012**, *111*, 07C708.

[23] Y. Saito, H. Takao, T. Tani, T. Nonoyama, K. Takatori, T. Homma, T. Nagaya, M. Nakamura, *Nature* **2004**, *432*, 84.

[24] K. Koyama, T. Sakuma, S. Yamamichi, H. Watanabe, H. Aoki, S. Ohya, Y. Miyasaka, T. Kikkawa, *Electron Devices Meet. 1991. IEDM '91. Tech. Dig. Int.* **1991**, 823.

[25] M. M. Watt, P. Woo, A. Kassam, G. Corporation, B. M. Melnick, S. Corporation, *Proc. Elev. IEEE Int. Symp. Appl. Ferroelectr.* **1998**, 11.

[26] M. Scigaj, N. Dix, I. Fina, R. Bachelet, B. Warot-Fonrose, J. Fontcuberta, F. Sánchez, *Appl. Phys. Lett.* **2013**, *102*, 112905.

[27] S. R. Singamaneni, W. Fan, J. T. Prater, J. Narayan, *J. Appl. Phys.* **2014**, *116*, 224104.

[28] C. Marchiori, M. Sousa, A. Guiller, H. Siegwart, J.-P. Locquet, J. Fompeyrine, G. J. Norga, J. W. Seo, *Appl. Phys. Lett.* **2006**, *88*, 072913.

[29] C. Xiong, W. H. P. Pernice, J. H. Ngai, J. W. Reiner, D. Kumarh, F. J. Walker, C. H. Ahn, H. X. Tang, *Nano Lett.* **2014**, *14*, 1419.

[30] C. Dubourdieu, J. Bruley, T. M. Arruda, A. Posadas, J. Jordan-Sweet, M. M. Frank, E. Cartier, D. J. Frank, S. V Kalinin, A. A. Demkov, V. Narayanan, *Nat. Nanotechnol.* **2013**, *8*, 748.

[31] D. C. Worledge, G. Hu, D. W. Abraham, J. Z. Sun, P. L. Trouilloud, J. Nowak, S. Brown, M. C. Gaidis, E. J. O'Sullivan, R. P. Robertazzi, *Appl. Phys. Lett.* **2011**, *98*, 022501.

[32] Y.-H. Wang, W.-C. Chen, S.-Y. Yang, K.-H. Shen, C. Park, M.-J. Kao, M.-J. Tsai, *J. Appl. Phys.* **2006**, *99*, 08M307.

[33] A. Vailionis, H. Boschker, W. Siemons, E. P. Houwman, D. H. A. Blank, G. Rijnders, G. Koster, *Phys. Rev. B* **2011**, *83*, 064101.

[34] G. Bayreuther, M. Dumm, B. Uhl, R. Meier, W. Kipferl, *J. Appl. Phys.* **2003**, *93*, 8230.

[35] L. Aballe, M. Foerster, E. Pellegrin, J. Nicolas, S. Ferrer, *J. Synchrotron Radiat.* **2015**, *22*, 745.

[36] I. Fina, L. Fábrega, E. Langenberg, X. Marti, F. Sánchez, M. Varela, J. Fontcuberta, *J. Appl. Phys.* **2011**, *109*, 074105.

[37] a) W. J. Merz, Phys. Rev. 1954, *95*, 690. b) C. F. Pulvari, W. Kuebler, *J. Appl. Phys.* **1958**, *29*, 1315.

[38] I.-W. Chen, Y. Wang, *Appl. Phys. Lett.* **1999**, *75*, 4186.

[39] A. Picinin, M. H. Lente, J. A. Eiras, J. P. Rino, *Phys. Rev. B* **2004**, *69*, 064117.

[40] D. J. Jung, K. Kim, J. F. Scott, *J. Phys. Condens. Matter* **2005**, *17*, 4843.

[41] M. Dawber, K. M. Rabe, J. F. Scott, *Rev. Mod. Phys.* **2005**, *77*, 1083.

[42] S. Sahoo, S. Polisetty, C.-G. Duan, S. S. Jaswal, E. Y. Tsymbal, C. Binek, *Phys. Rev. B* **2007**, *76*, 092108.

[43] W.-G. Wang, M. Li, S. Hageman, C. L. Chien, *Nat. Mater.* **2011**, *11*, 64.

[44] C. Burrowes, N. Vernier, J.-P. Adam, L. Herrera Diez, K. Garcia, I. Barisic, G. Agnus, S. Eimer, J.-V. Kim, T. Devolder, A. Lamperti, R. Mantovan, B. Ockert, E. E. Fullerton, D. Ravelosona, *Appl. Phys. Lett.* **2013**, *103*, 182401.

[45] Ferré, in *Spin Dyn. Confin. Magn. Struct. I, Top. Appl. Phys.* (Eds.: B. Hillebrands, K. Ounadjela), Springer-Verlag, Berlin Heidelberg, **2002**, pp. 127–165.

[46] E. Y. Tsymbal, *Nat. Mater.* **2012**, *11*, 12.

[47] H. L. Stadler, *J. Appl. Phys.* **1962**, *33*, 3487.

[48] M. H. Yeh, Y. C. Liu, K. S. Liu, I. N. Lin, J. Y. M. Lee, H. F. Cheng, *J. Appl. Phys.* **1993**, *74*, 2143.

[49] G. Bertotti, *Hysteresis in Magnetism*, Academic Press, San Diego, CA, USA, **1998**.

[50] R. Skomski, R. D. Kirby, D. J. Sellmyer, *J. Appl. Phys.* **2003**, *93*, 6820.

[51] P. Gaunt, *Philos. Mag.* **1976**, *34*, 775.

[52] G. Radaelli, S. Brivio, I. Fina, R. Bertacco, *Appl. Phys. Lett.* **2012**, *100*, 102904.

[53] R. Bertacco, M. Cantoni, M. Riva, A. Tagliaferri, F. Ciccacci, *Appl. Surf. Sci.* **2005**, *252*, 1754.

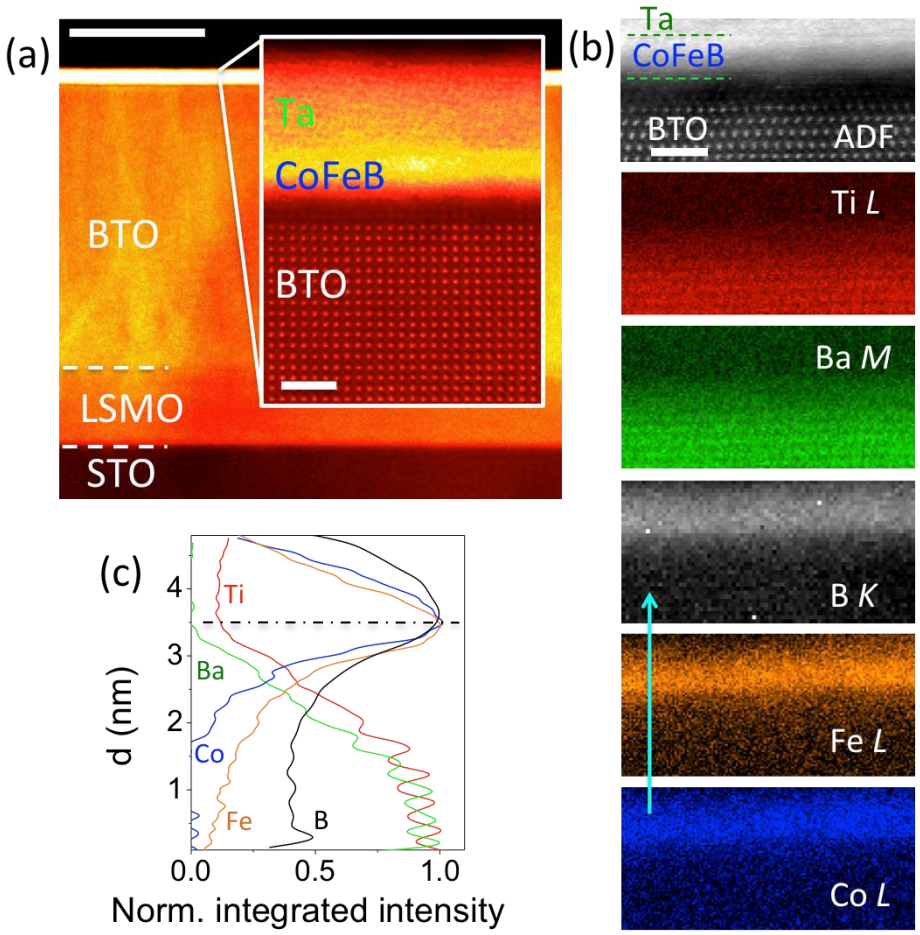

Figure 1. (a) STEM images from a Ta(2.5)/CoFeB(1.1)/BTO(100)/LSMO(30)/STO stack (thickness in nm). The scale bar is 50 nm. Dashed horizontal lines mark the interface positions, and the different layers are identified accordingly. The inset exhibits atomic resolution images of BTO/CoFeB/Ta interfaces. The scale bar is 2 nm. (b) EELS elemental maps across the Ta/CoFeB/BTO region shown in the top panel, acquired in Annular Dark Field imaging mode (ADF). The scale bar is 2 nm. (c) Averaged signals for B, Ti, Fe, Co and Ba across the stack, taken along the direction indicated by the light blue arrow in panel b. Dashed green lines in the top panel indicate the two boundaries of the CoFeB layer.

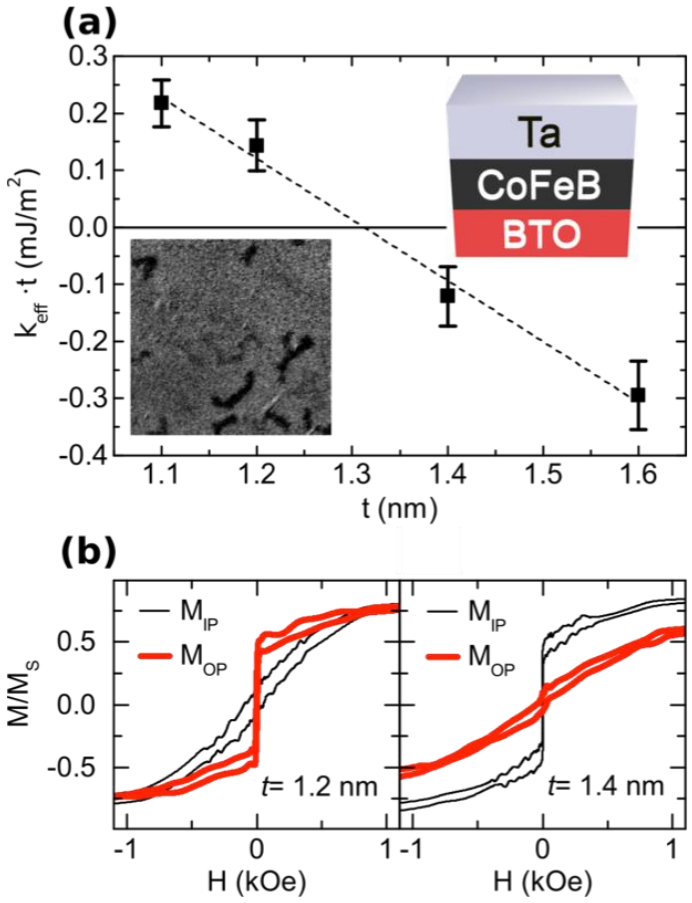

Figure 2. (a) Effective anisotropy energy per unit surface versus CoFeB thickness (*t*) in unpatterned STO/BTO/CoFeB/Ta multilayers, as determined by VSM. Positive values below 1.3 nm indicate an out-of-plane easy axis. In the left-bottom inset, a XPEEM image of CoFeB in an out-of-plane magnetic remanent state is shown. (b) Zoom of VSM loops for the magnetization component parallel to the applied magnetic field, in a region around the remanence condition. The in-plane (black narrow line) and out-of-plane (red thick line) loops are reported, for a 1.2 nm thick CoFeB layer with PMA (left) and a 1.4 nm thick layer with easy plane anisotropy (right). The in-plane (M_{IP}) and out-of-plane (M_{OP}) components are normalized to the saturation magnetization (M_S).

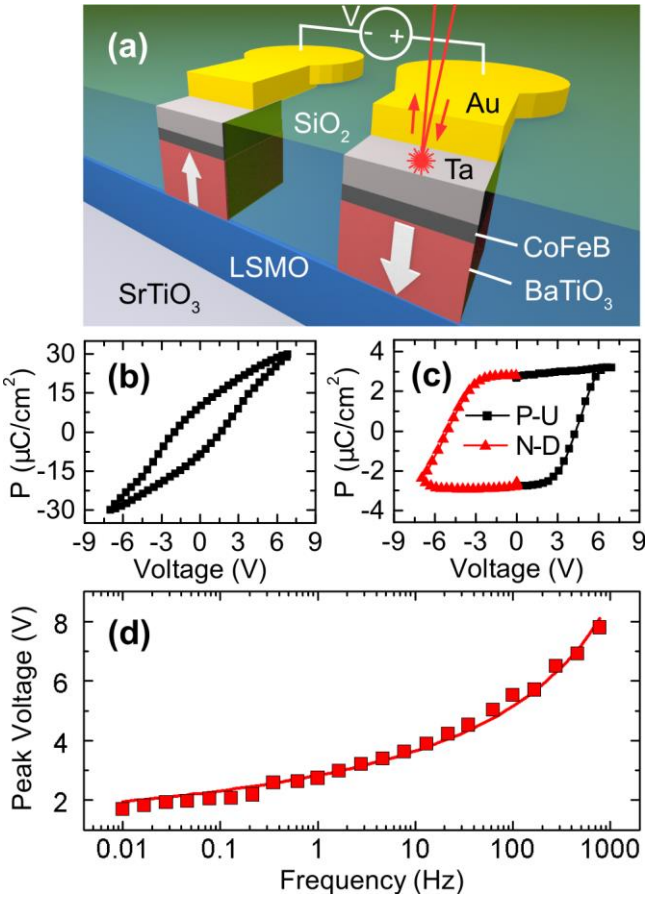

Figure 3. (a) Sketch of the micro-capacitors used for the ferroelectric and magneto-electric characterization. (b) Ferroelectric Dynamic Hysteresis Loop recorded on a micro-capacitor at a frequency of 200 Hz with Dynamic Leakage Current Compensation. (c) Positive-Up Negative-Down (PUND) measurement at 100 Hz. P is the FE polarization. (d) Frequency dependence of the ferroelectric coercive voltage, corresponding to the voltage of the switching current peak during PUND measurements at variable frequency. The red line is a fit with the Merz equation.

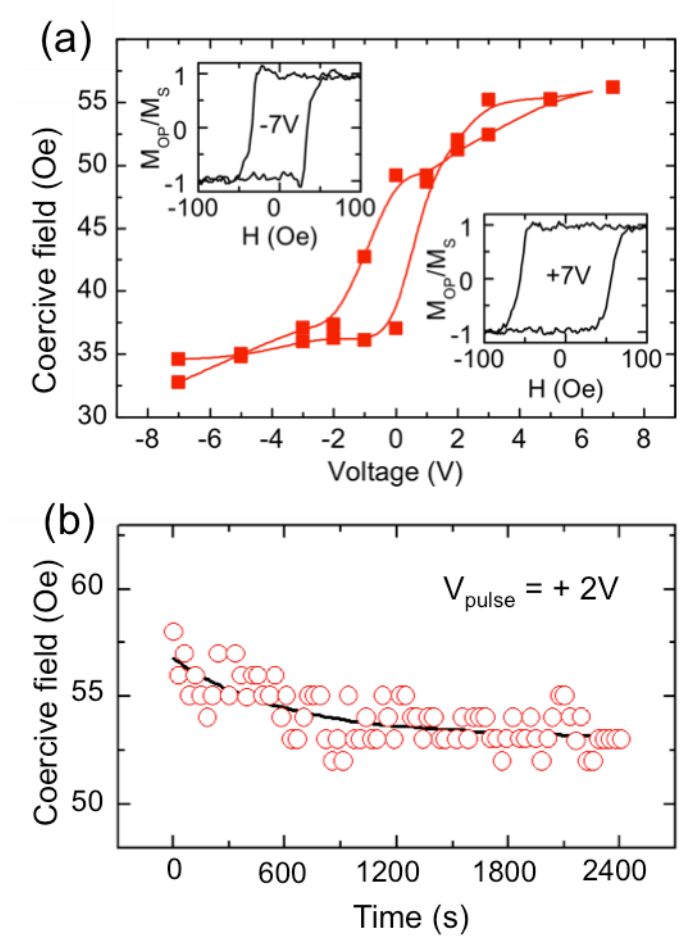

Figure 4. (a) Hysteretic behavior of the out-of-plane magnetic coercive field (red squares) of the CoFeB layer as a function of the applied voltage across the capacitor. The red line is a guide to the eye. Examples of polar MOKE loops for ±7 V applied across the capacitor are shown as insets. (b) Stability of the high coercivity magnetic state set by application of a voltage pulse of +2 V. The black line is an exponential fit with a time constant of ~ 500 s.

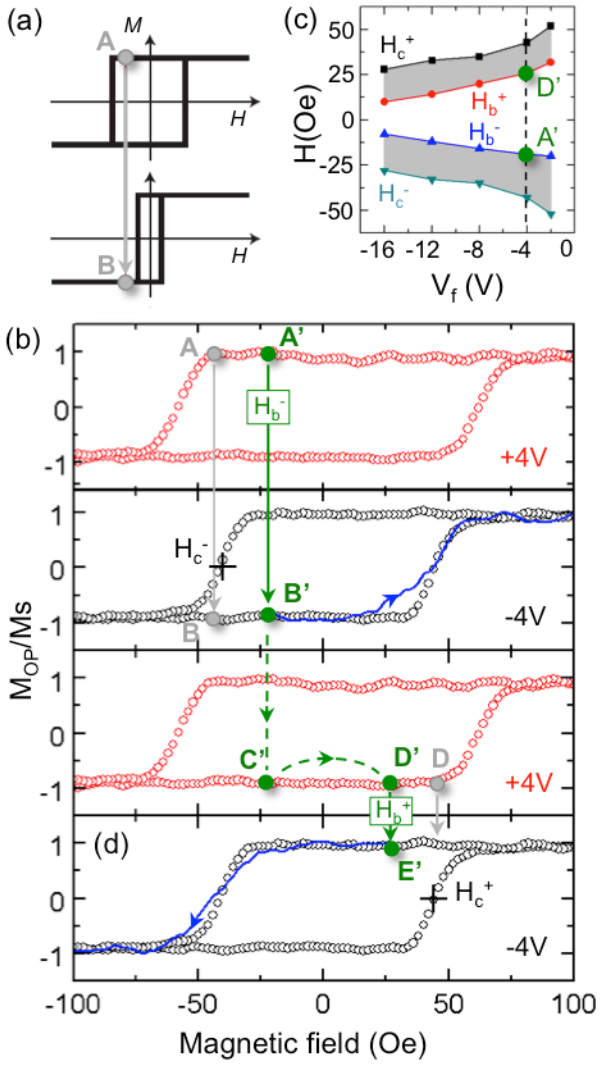

Figure 5. (a) Sketch of the mechanism leading to magnetic flip upon electrically induced shrinking of the magnetic hysteresis loop. (b) Demonstration of a reversible magnetization flip. The up-down magnetization flip (A-B or A'- B' transitions) is induced by switching the applied voltage across the capacitor from V_S= +4 V to V_f = -4 V under a uniform bias magnetic field H_b. Both the voltage and bias field are then reversed so as to prepare an initial state between D' and D. Finally the down-up transition (e.g. D'-E') is achieved by switching again the voltage to V_f = -4V. Green symbols and letters refer to the minimum bias field ($H_b^{\pm}$) needed to ensure a magnetic flip within 2 s from the electric switching. (c) Minimum magnetic bias fields required for the up-down (H_b^-) and down-up (H_b^+) magnetic flip at a given value of the switching voltage V_f, compared with the coercive magnetic field in the low coercive state ($H_c^{\pm}$). The shaded areas indicate the anomalous transitions according to the general scheme of panel (a).

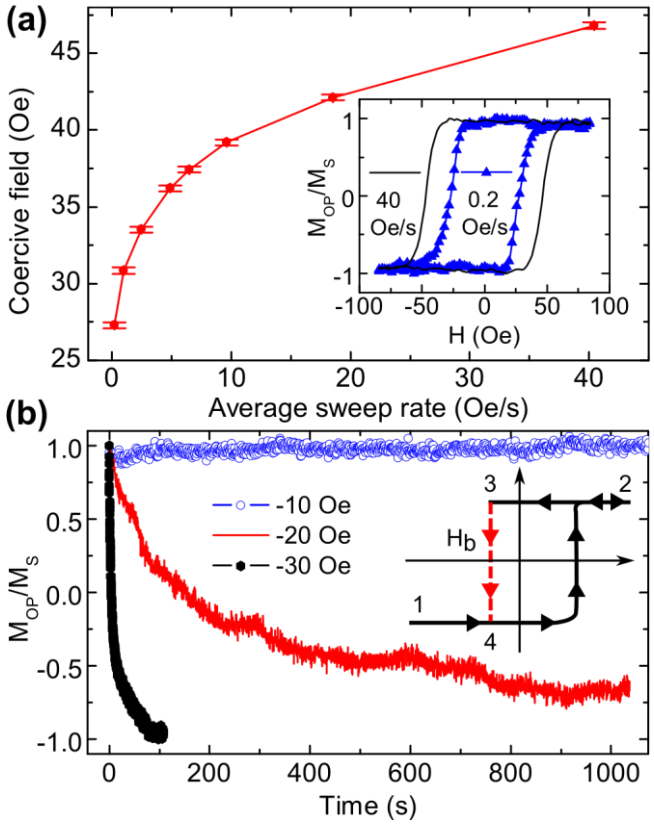

Figure 6. (a) Magnetic coercive field of the CoFeB layer, as measured with MOKE, versus the average sweep rate of the magnetic field. The field was increased in steps of 2 Oe with a dwell time consistent with the average sweep rate reported in figure. In the inset two hysteresis loops recorded at 40 Oe/s (continuous line) and 0.1 Oe/s (triangles) are shown. (b) Magnetic relaxation curves measured by MOKE after preparation of the initial up state at a negative magnetic field H_b, according to the protocol sketched in the inset. First the sample is saturated in the up state following the 1-2 portion of the hysteresis loop. Then the field is reduced and reversed till to achieve H_b , at a sweep rate of 40 Oe/s, and the relaxation (3-4) is recorded.

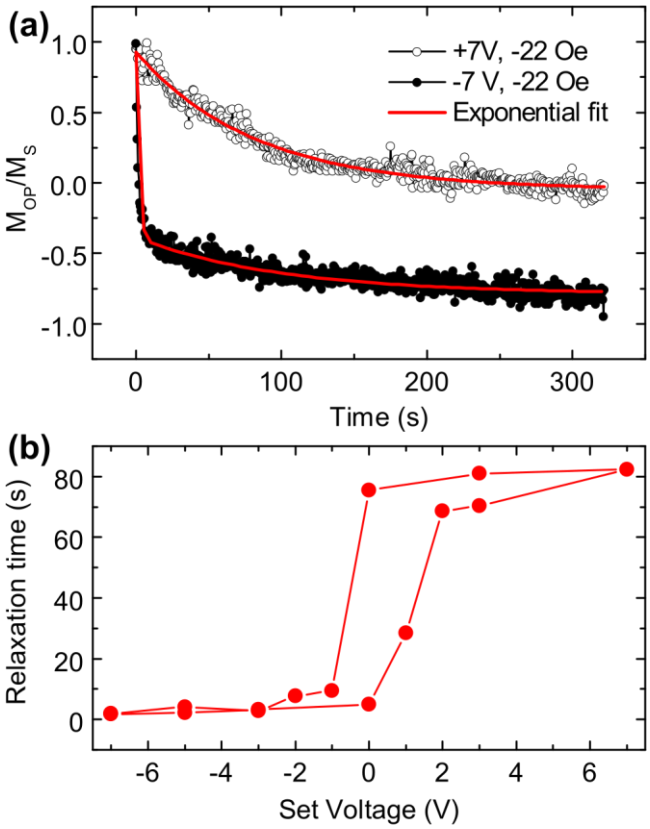

Figure 7. (a) Magnetic relaxation curves recorded at H_b= -22 Oe for opposite values of the applied voltage across the capacitor. The experimental data were fitted by bi-exponential curves. For -7 V both the fast and slow components are clearly seen while at +7 V the slow component is negligible in this time window (see. the Supporting Information for details on the fit). (b) Relaxation times associated to the fast component of the relaxation curves versus the applied voltage, at fixed H_b= -22 Oe.

Supporting Information

Electrical Switching of Magnetization in the Artificial Multiferroic System $Co_{0.4}Fe_{0.4}B_{0.2}/BaTiO_3$: the Role of Magnetic Viscosity

*L.Baldrati,[1] Dr. C. Rinaldi,[1,2] A. Manuzzi,[1] M. Asa,[1] S. Bertoli,[1] Dr. L. Aballe,[3] Dr. M. Foerster,[3] N. Biškup,[4,5] Prof. M. Varela,[4] Prof. M. Cantoni,[1] Prof. R. Bertacco[1,2]**

[1]*Department of Physics, Politecnico di Milano, Via G. Colombo 81, 20133, Milano, Italy*
[2]*IFN-CNR, Via G. Colombo 81, 20133 Milano, Italy*
[3]*ALBA Synchrotron Light Facility, Carretera BP 1413, Km. 3.3, Cerdanyola del Vallès, Barcelona 08290, Spain*
[4]*GFMC & Instituto Pluridisciplinar, Universidad Complutense de Madrid, Madrid, 28040, Spain*
[5]*Centro Nacional de Microscopía Electrónica, Universidad Complutense de Madrid, Madrid, 28040, Spain*

E-mail: riccardo.bertacco@polimi.it

STEM analysis on as grown samples

Figure S1 reports Scanning transmission electron microscopy (STEM) images taken from an as-grown Ta(2.5)/CoFeB(1.1)/BTO(100)/LSMO(30)/STO stack (thickness in nm), displaying easy-plane magnetic anisotropy.

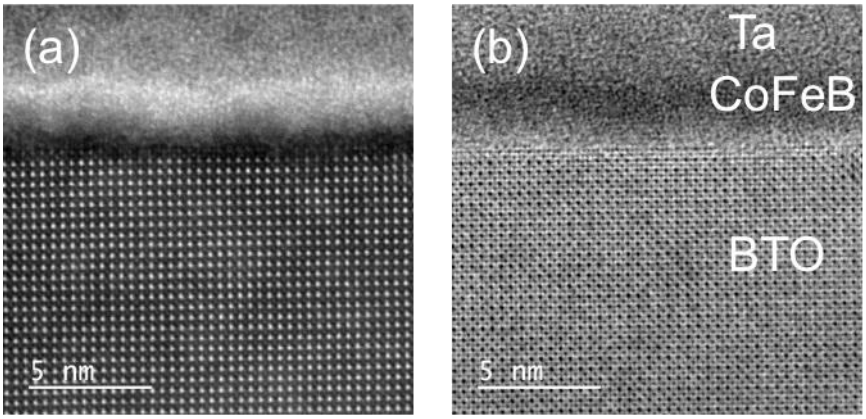

Figure S1: STEM images from a not annealed stack: (a) Z-contrast (high angle annular dark field image) and (b) annular bright field image.

The main difference with respect to samples annealed at 250 °C to promote PMA is the much higher corrugation of the CoFeB film (see Figure 1 of the main text for comparison).

Unfortunately, this corrugation prevents a reliable EELS analysis across the interface and a quantitative assessment of the impact of the annealing on the B interdiffusion in the heterostructure.

XPEEM investigation

X-PEEM measurements have been performed to investigate the magnetic domain structure of CoFeB with perpendicular to plane anisotropy in micro-capacitors patterned on Ta(2.5)/CoFeB(1.1)/BTO(100)/LSMO(30)/STO stacks (thickness in nm) annealed at 250 °C in a magnetic field of 4 kOe perpendicular to plane. The photon beam was focused on the sample down to a 12x36 μm^2 footprint, at an angle of incidence of 16 degrees with respect to the sample surface. As the XMCD contrast is proportional to $cos(\theta)$, where θ is the angle between the direction of the magnetization and the circularly polarized beam, the setup in this geometry is more sensitive to the in-plane component of the magnetization. However, also the out-of-plane component can be detected, as $cos(\theta) = 0.28$ in our case. Figure S2a shows the X-ray Absorption Spectra (XAS) in the region of the Fe and Co L_{32} edge with a visible signal from Ba of the underlying BTO. The XAS peak shape resembles that of metallic Fe and Co with some additional feature/shoulder at the high energy side which are also found in the corresponding alloys with Boron, while we note the absence of signs of significant oxidation.[1] X-PEEM images have been recorded at the Fe L_3 edge in different magnetic configurations. Figure S2b shows space-resolved XMCD contrast at remanence, after the application of -110 Oe bias field (pointing inwards with respect to the sample surface) along the direction perpendicular to the plane of the sample. A few dark domains showing a labyrinth pattern structure, typical of perpendicularly magnetized samples, are observed. Upon application of +110 Oe in the opposite direction we clearly see that worm-like dark domains increase in number, covering more or less half of the sample area. Despite the setup was mainly sensitive to the in-plane component of magnetization, the observed behavior upon application of out-of-plane magnetic

fields, in addition to the observed domain shapes which are characteristic of PMA materials, strongly suggests that black area in the XMCD maps can be associated to domains with magnetization pointing outwards, while brighter areas correspond to domains with inwards magnetization. This is consistent with the MOKE analysis of our samples and reveals the tendency of the sample to break in domains, whose expansion via domain wall motion is the main mechanism responsible for magnetization reversal. Upon application of -110 Oe (Fig. S2b) the sample appears mainly bright, thus indicating good ferromagnetic remanence with inwards magnetization, while the 50% ratio between dark and bright domains in Fig. S2c, upon application of +110 Oe, shows a sizable magnetization reversal, even though not complete. As the maps of Fig. S2b and S2c have been take in sequence, we attribute the reduced remanence for positive fields to the progressive sample damage under the X-ray beam, which tends to de-stabilize the PMA.

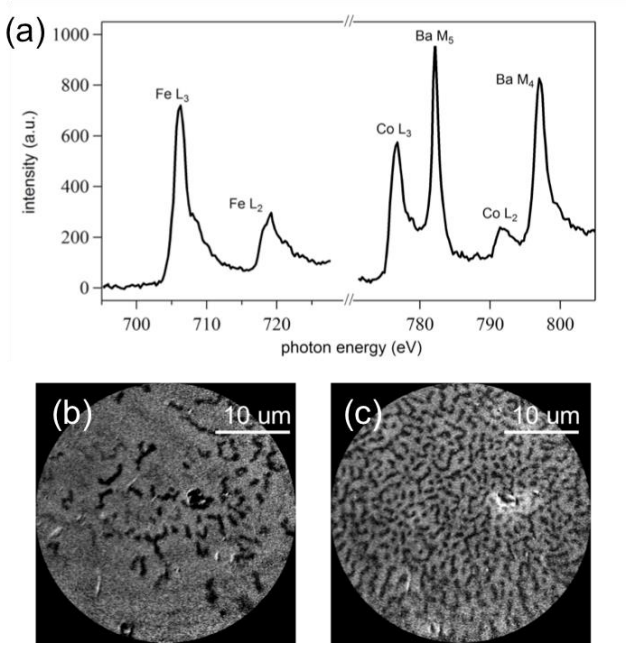

Figure S2. (a) X-ray absorption spectrum (XAS) of the CoFeB in patterned devices. (b) X-PEEM image of CoFeB. The image is acquired at remanence, after the application of -110 Oe (inwards). (c) As in (b) but in remanence, upon application of +110 Oe (outwards, with respect to the sample surface).

Insensitivity to the underlying LSMO layer in polar MOKE experiments and relevance of the annealing to achieve PMA

Since the probing depth of visible light in metals is in the order of 10 nm, the Kerr rotation measured by MOKE on our micro-capacitors is in general the weighted sum of the CoFeB and LSMO contributions. In order to distinguish and quantify these two contributions, we have tracked the magnetic properties of a sample (Ta(1.5)/CoFeB(1.1)/ BTO(150)/LSMO(50)/STO) (thickness in nm) during the main steps of growth and post-annealing. In Figure S3 we present longitudinal (panel a) and polar (panel b) MOKE data taken on (i) the BTO/LSMO bilayer as-grown by PLD (open dots), (ii) the complete stack including the bilayer Ta/CoFeB grown by sputtering (red cross) and (iii) the same complete stack after 15 min annealing at 250 °C in a magnetic field of 4 kOe applied out-of-the plane (blue squares).

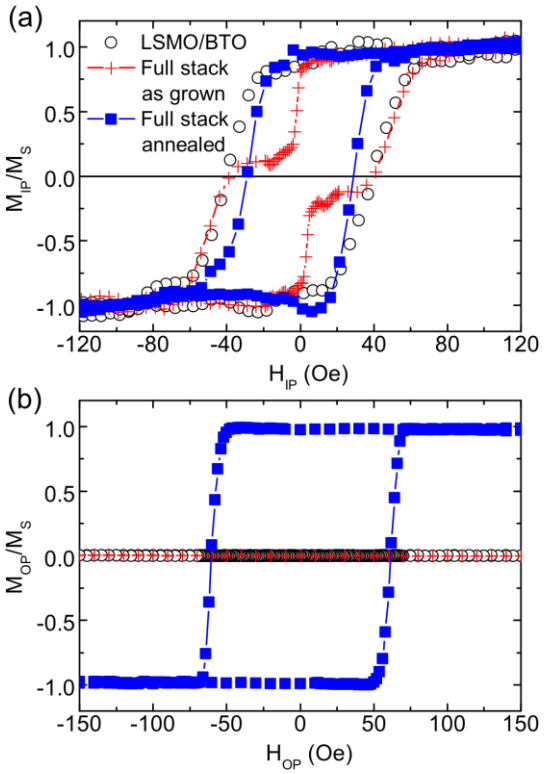

Figure S3. (a) Longitudinal MOKE ellipticity loops from: (i) the template BTO(150)/LSMO(50)/STO (black open circles), (ii) the as-grown complete heterostructure Ta(1.5)/CoFeB(1.1)/BTO(150)/LSMO(50)/STO (red crosses) and (iii) the same heterostructure after annealing at 250 °C for 15 min in a 4 kOe out-of-plane magnetic field (blue squares). (b) Polar MOKE loops of the same sample as in (a). No out-of-plane magnetic signal is detected before the annealing, while the CoFeB magnetization reorients out of the plane upon annealing.

The longitudinal MOKE (Figure S3a) of the BTO/LSMO bilayer on STO and the one of the full stack after the addition of the Ta/CoFeB bilayer show significantly different hysteresis loops. The former (black open circles) displays a single magnetic component with a coercive field of 40 Oe, attributed to LSMO, which is the only magnetic material in the structure. The latter, before annealing (red crosses), displays two components: the first one has a coercive field of 50 Oe (attributed to LSMO) while the second one has a coercive field of 3 Oe, attributed to the CoFeB with in-plane easy axis. The data after annealing (blue squares) display again a single magnetic component presenting a coercive field of 29 Oe, which we attribute to LSMO. The CoFeB contribution disappears since its magnetic anisotropy has reoriented out-of-plane. The polar MOKE (Figure S3b), on the other hand, presents no magnetic contribution from LSMO in the bare LSMO/BTO/STO structure (open circles). The LSMO layer does not display PMA, like the as grown CoFeB (red crosses) in the complete stack before the annealing. After annealing (blue squares), instead, the signal is dominated by the out-of-plane CoFeB magnetization. This analysis clearly demonstrates that polar MOKE loops from annealed samples presented in the main text only reflect the CoFeB magnetic properties and are insensitive to the LSMO layer.

Fitting magnetic relaxation data

Usually magnetic relaxation and viscosity phenomena are modeled assuming a uniform distribution of energy barriers of the systems, eventually leading to a logarithmic dependence of the magnetization vs. time for fixed bias field, according to the formula:[2,3]:

$$M(H_b,t) = M_0(H_b,t_0) - S\ln(t/t_0) \qquad \text{(Equation S1)}$$

An attempt to fit our data with the above model is presented in Figure S4. It is evident that a reasonable fit cannot be obtained by the logarithmic law described above, especially for the initial portion of the curve, where a fast relaxation takes place.

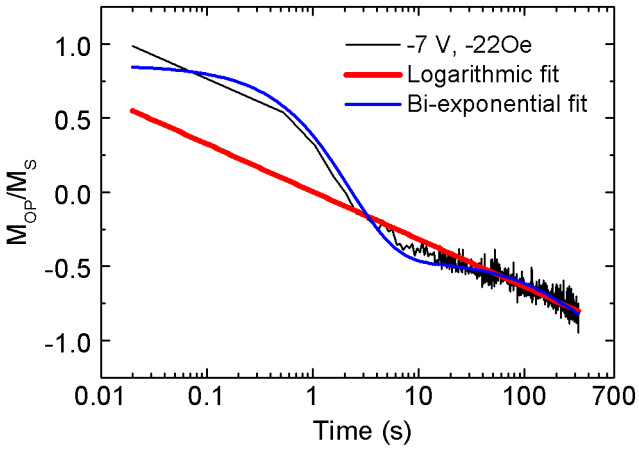

Figure S4. Comparison between logarithmic and bi-exponential fit of the experimental magnetic relaxation curve measured at -22 Oe, with an applied voltage of -7 V.

The simplest way to fit the raw data of Figure 7a in the main text is to use a bi-exponential function with a fast and slow component. This is the procedure adopted for fitting magnetic relaxation curves taken at different voltage in the main text. For positive voltages a single exponential, corresponding to the fast component, has been used. This is because in the reasonable observation window where instrumentation drifts and instabilities can be neglected (from 300 s to 500s) the long relaxation times at positive bias largely exceeds the observation window. Noteworthy, however, the amplitude of the fast and slow components are quite constant (within ±25%) for all voltage values where they are defined. This supports the physical soundness of the bi-exponential fit. Following the general treatment of magnetic relaxation we can suppose that the CoFeB film behaves as if it is made of two populations of poorly interacting grains with characteristic volumes V_1 and V_2. The electrically induced variation of perpendicular magnetic anisotropy modulates the energy barrier for the magnetic flip of the grains, thus giving rise to two characteristic exponential decays whose time constant is

$$t_{1,2} = t_0 \exp(KV_{1,2}/K_BT) \qquad \text{(Equation S2)}$$

where K is the effective PMA anisotropy constant, k_B the Boltzmann constant and τ_0 a characteristic time of the system.

Even though TEM data reveal some film granularity for the CoFeB layer, so far, we do not have structural data allowing to determine independently the existence of the above mentioned size distribution. The observed bi-exponential behavior could be also associated with the existence of two relevant activation energies for the nucleation of domains and/or the depinning of domain walls during magnetization reversal. As a matter of fact for nucleation-dominated reverse processes the relaxation is expected to be described by a sum of exponential events, [4] leading to concave curves like those in Figure 7a of the main text. A full understanding of the physical origin of the bi-exponential behavior is relevant for the minimization of magnetic viscosity and relaxation times, but this is beyond the scope of this work.

REFERENCES

[1] P. V. Paluskar, R. Lavrijsen, M. Sicot, J. T. Kohlhepp, H. J. M. Swagten, B. Koopmans, *Phys. Rev. Lett.* **2009**, *102*, 016602.

[2] G. Bertotti, *Hysteresis in Magnetism*, Academic Press, San Diego, CA, USA, **1998**.

[3] R. Skomski, R. D. Kirby, D. J. Sellmyer, *J. Appl. Phys.* **2003**, *93*, 6820.

[4] J. Ferré, in *Spin Dyn. Confin. Magn. Struct. I*, *Top. Appl. Phys.* (Eds.: B. Hillebrands, K. Ounadjela), Springer-Verlag, Berlin Heidelberg, **2002**, pp. 127–165.